Electronic Supplementary Material (ESI) for Energy & Environmental Science.

Supporting Information

Coupling of Indium Clusters with Atomic Fe-N_4 on Carbon for Long-term Rechargeable Zn-Air Batteries

Xinxin Shu, Xueying Cao, Bowen He, XunYi Chen, Lanling Zhao, Chengdong Yang, Jizhen Ma, and Jintao Zhang*

Key Laboratory for Colloid and Interface Chemistry of State Education Ministry, School of Chemistry and Chemical Engineering, Shandong University, Jinan 250100

*Corresponding Author(s): jtzhang@sdu.edu.cn

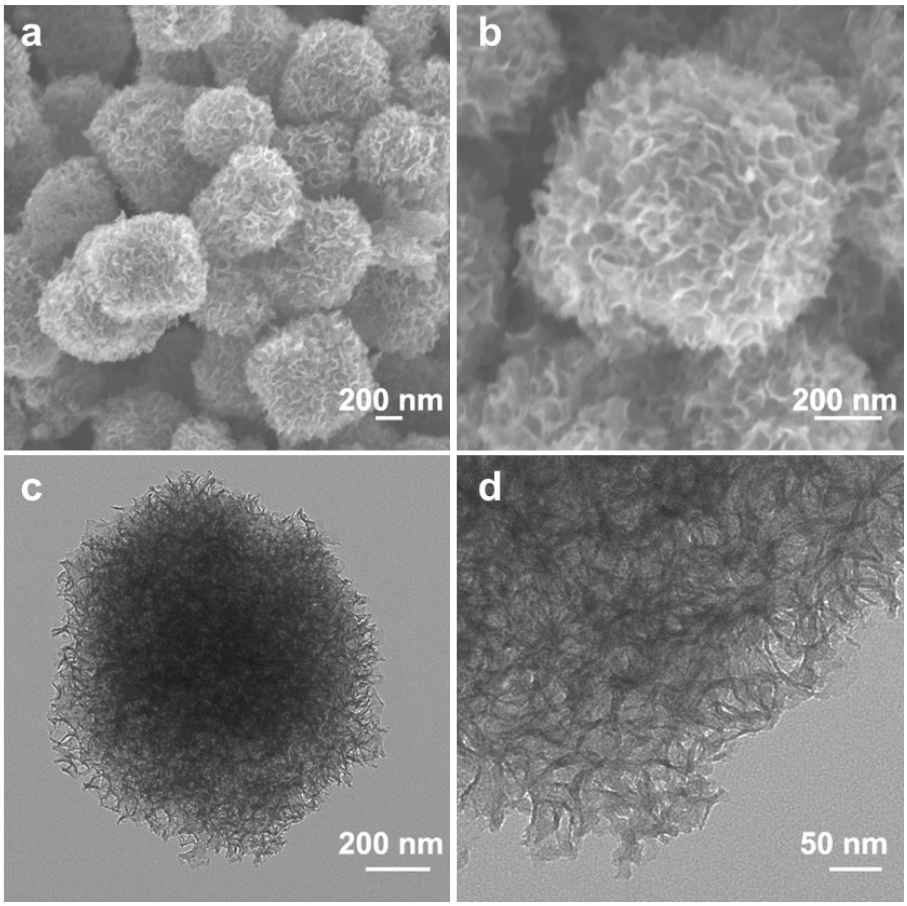

Figure S1 (a, b) SEM images and (c, d) TEM images of In/NC samples.

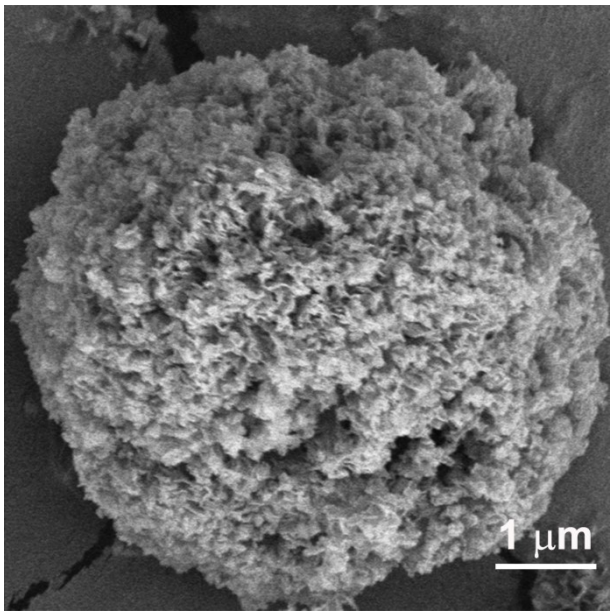

Figure S2 The SEM image of folic acid and melamine (FM) supermolecules.

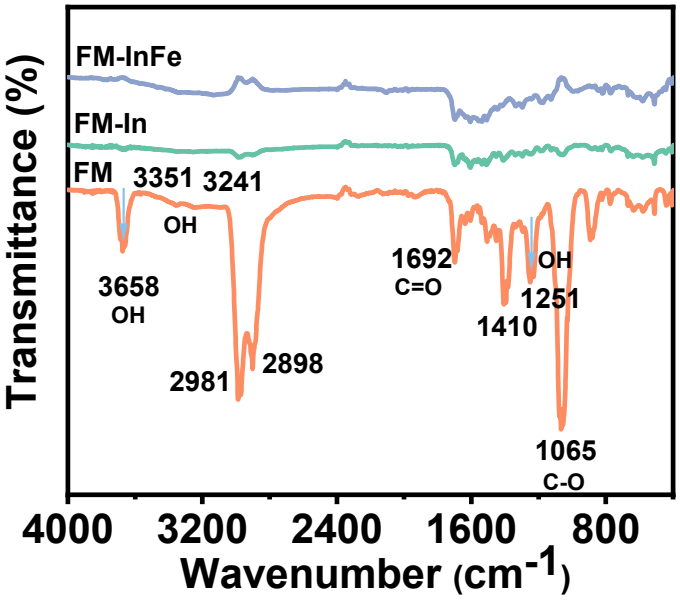

Figure S3 The Fourier transform infrared spectrum of FM, FM-In and FM-InFe supermolecules.

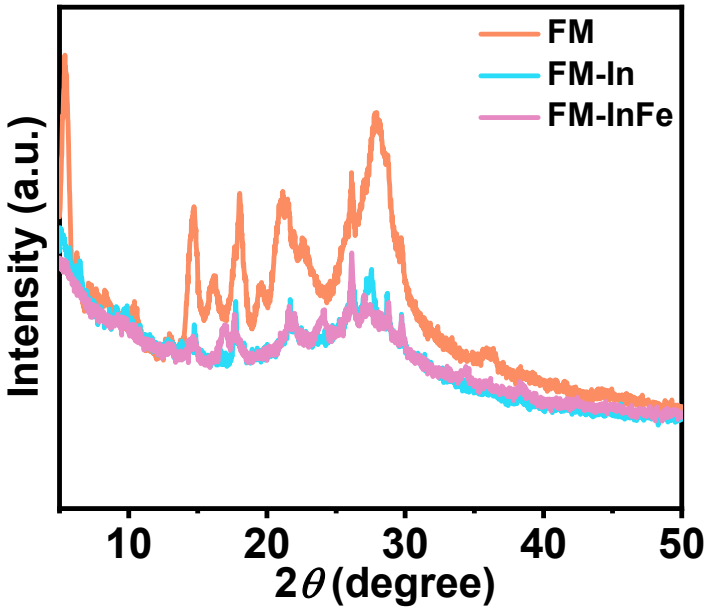

Figure S4 The XRD patterns of FM, FM-In, and FM-InFe supermolecules.

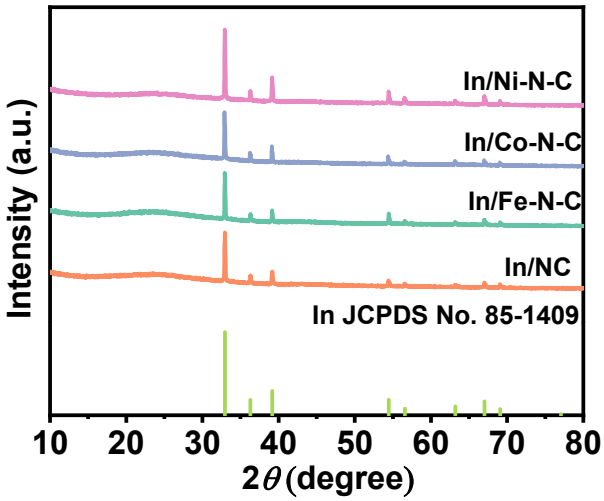

Figure S5 XRD patterns of In/NC, In/Fe-N-C, In/Co-N-C, and In/Ni-N-C samples.

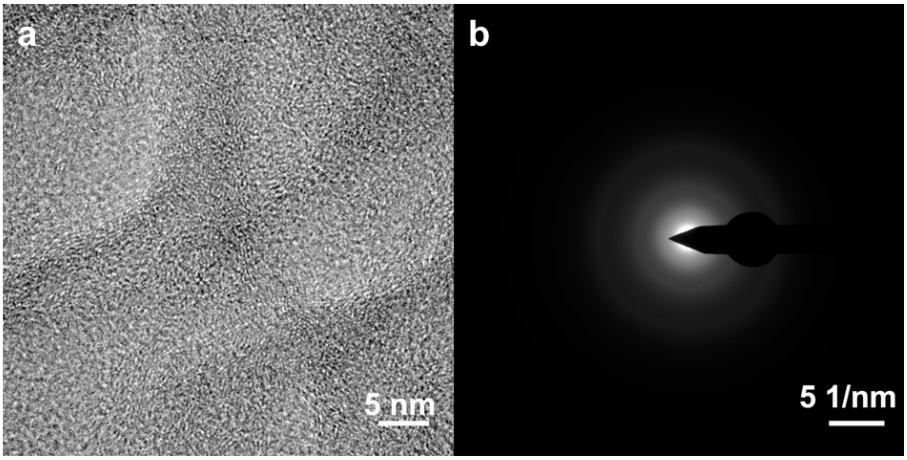

Figure S6 (a) High-resolution TEM image and (b) the selection electron diffraction diagram of In/Fe-N-C sample.

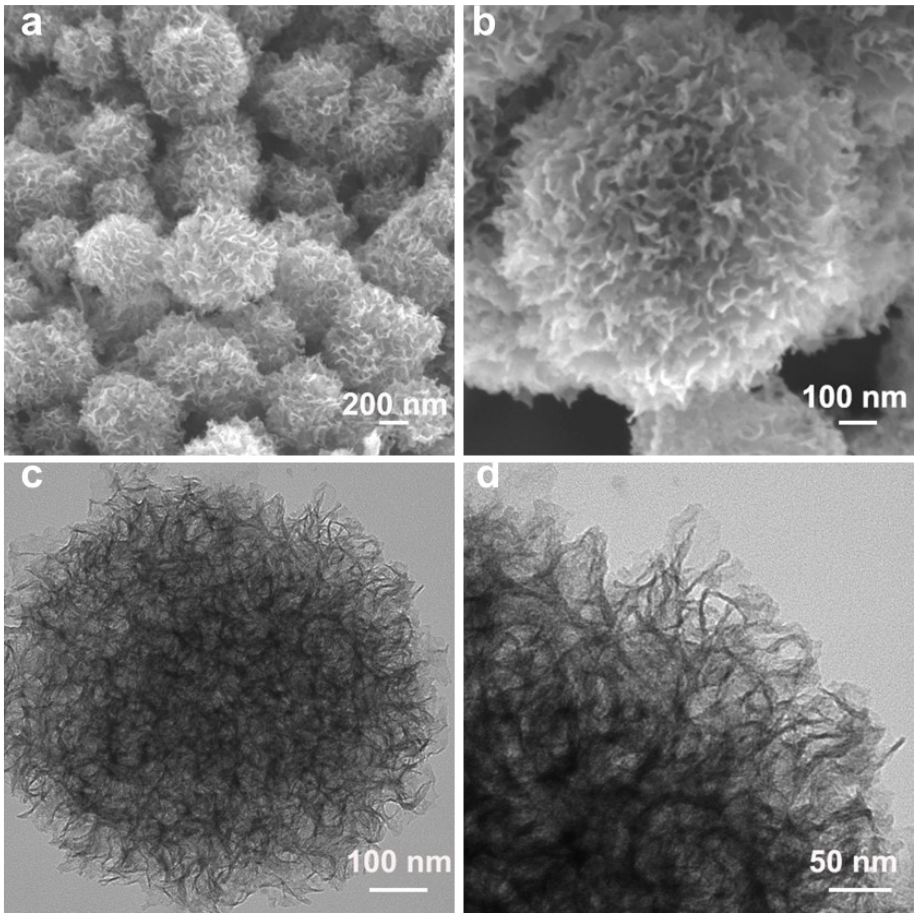

Figure S7 (a, b) The SEM images and (c, d) the TEM images of In/Co-N-C samples.

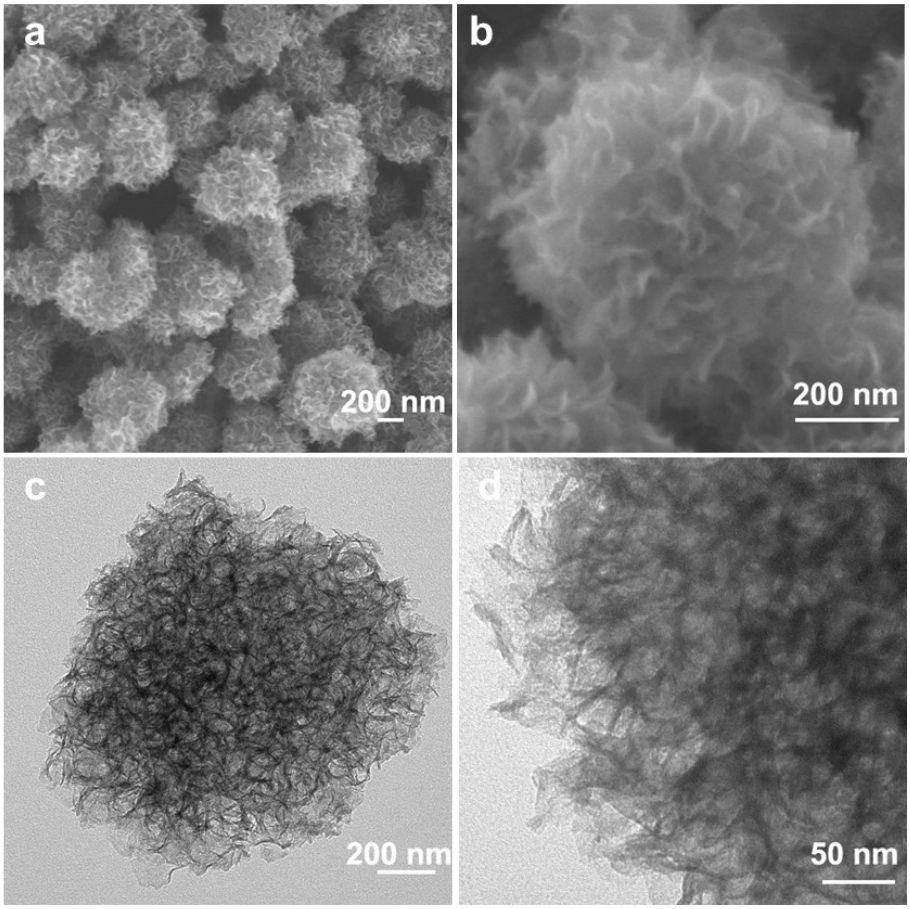

Figure S8 (a, b) The SEM images and (c, d) the TEM images of In/Ni-N-C samples.

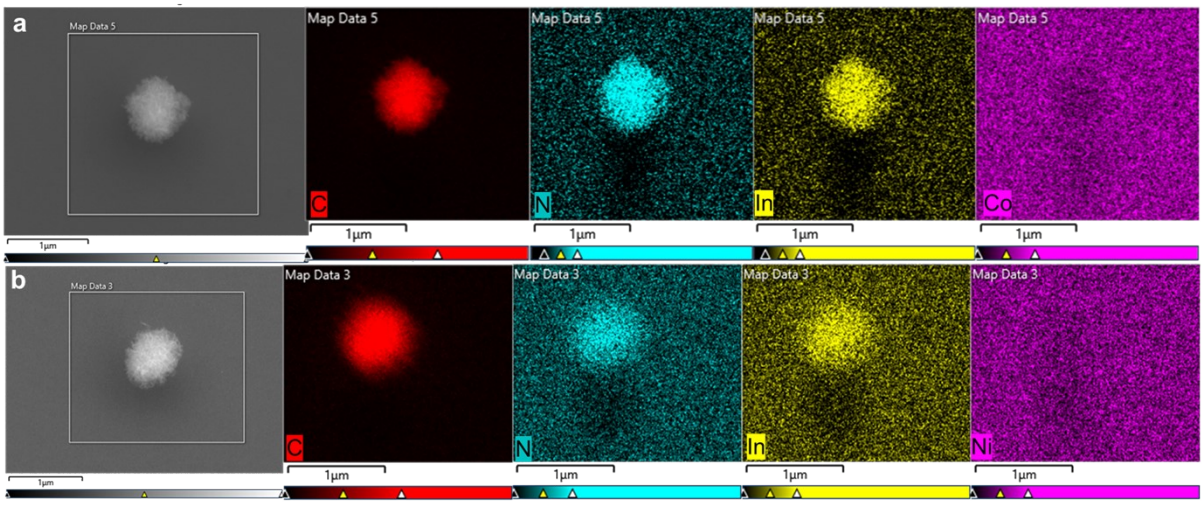

Figure S9 The mapping images of (a) In/Co-N-C and (b) In/Ni-N-C.

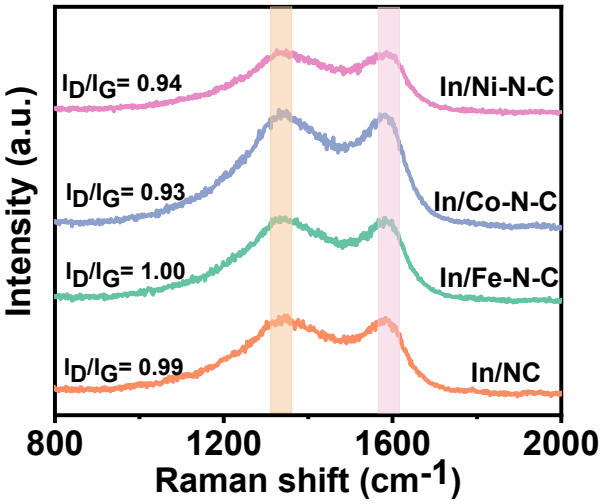

Figure S10 Raman spectra of In/NC, In/Fe-N-C, In/Co-N-C, and In/Ni-N-C samples.

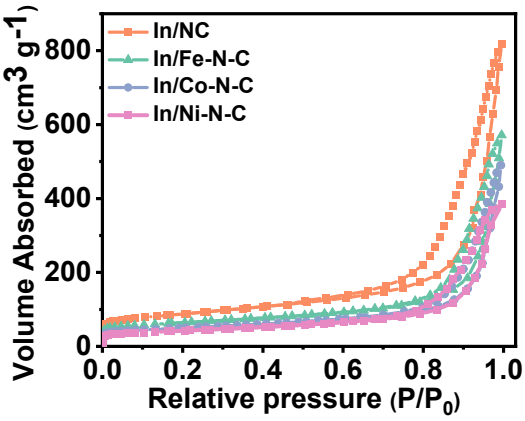

Figure S11 The nitrogen absorption and desorption curves.

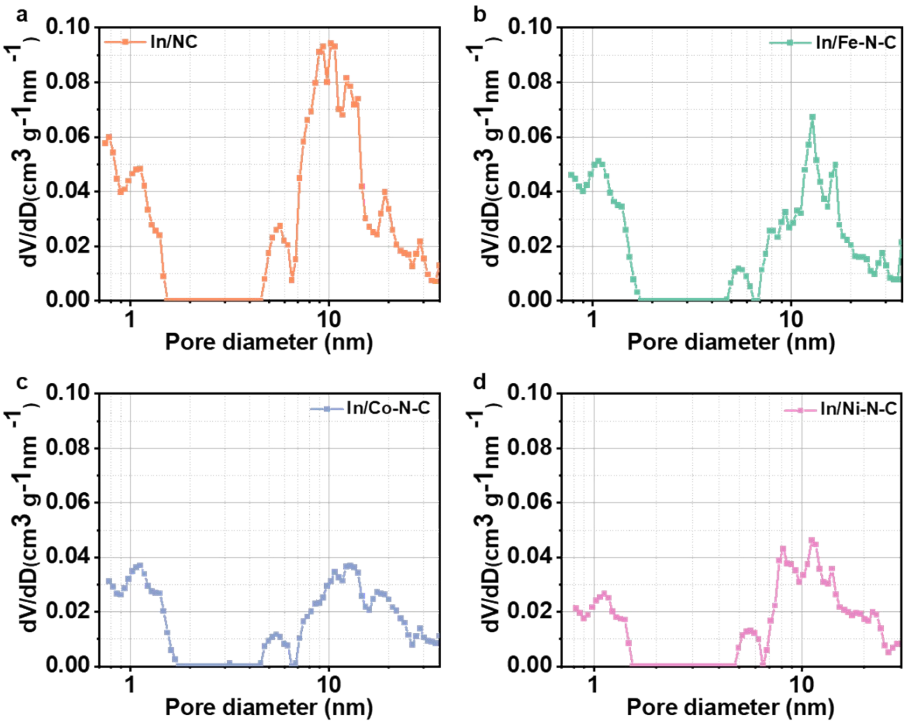

Figure S12 Pore size distribution diagrams of In/NC, In/Fe-N-C, In/Co-N-C and In/Ni-N-C catalysts.

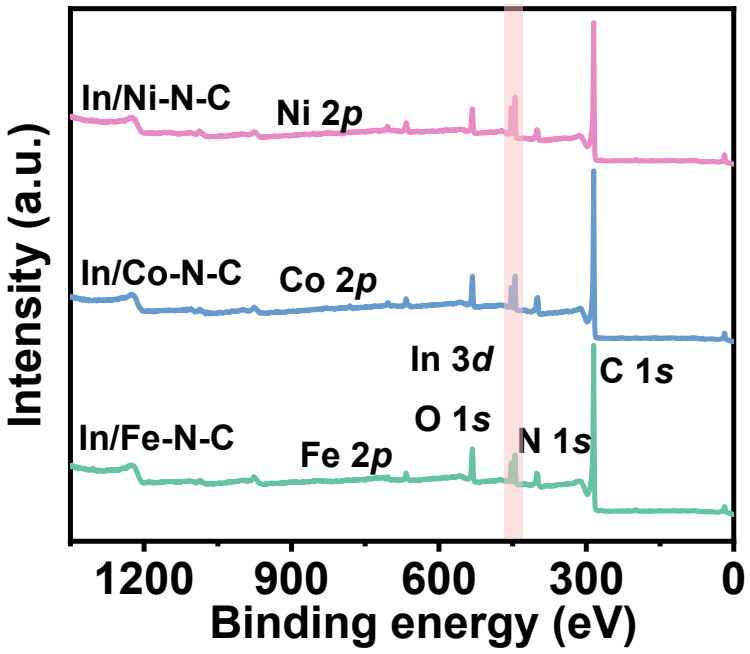

Figure S13 XPS survey spectrum.

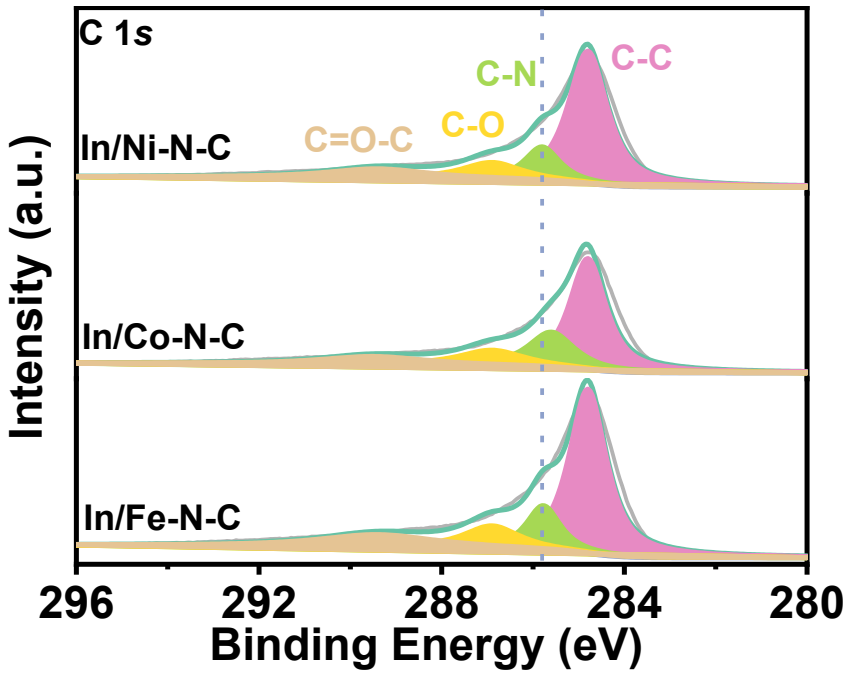

Figure S14 The C1*s* XPS spectra.

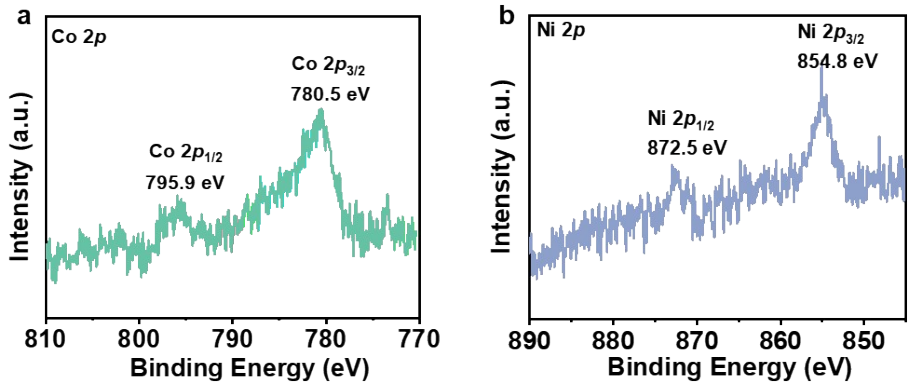

Figure S15 (a) The Co 2*p* XPS spectra of In/Co-N-C. (b) The Ni 2*p* XPS spectra of In/Ni-N-C.

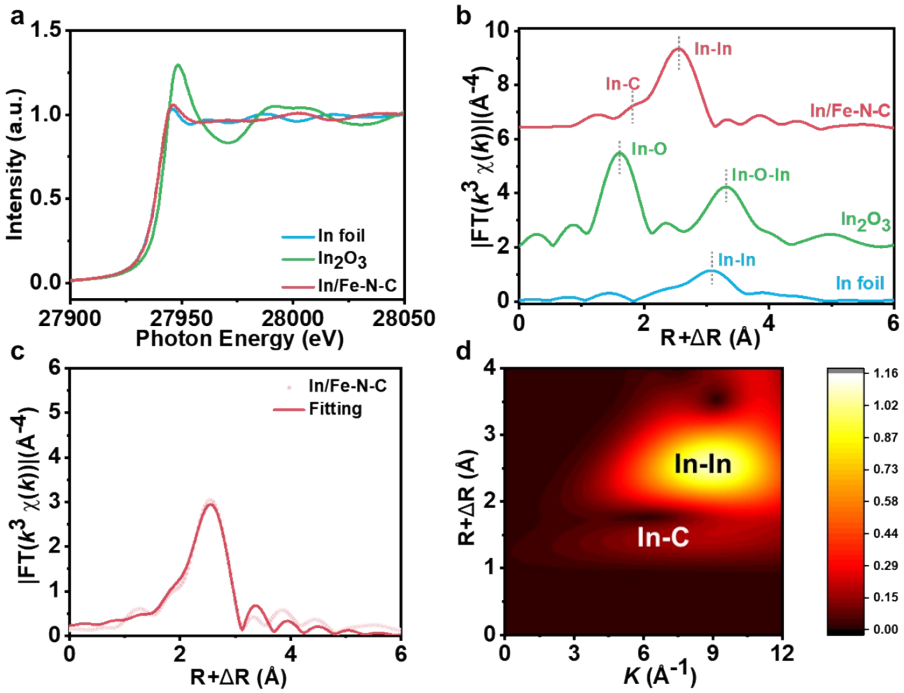

Figure S16 (a) In K-edge XANES spectra of In/Fe-N-C, In foil and In_2O_3. (b) In K-edge FT-EXAFS spectra of In/Fe-N-C, In foil and In_2O_3. (c) FT-EXAFS fitting curve of In/Fe-N-C. (d) WT-EXAFS plots of In/Fe-N-C.

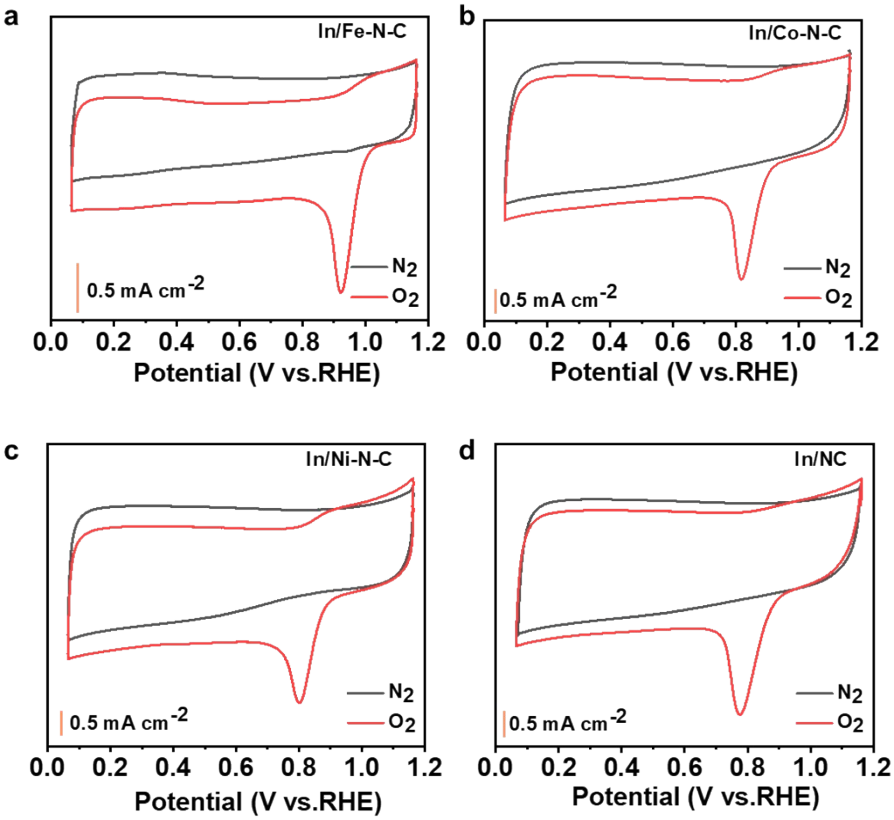

Figure S17 CV curves of (a) In/Fe-N-C, (b) In/Co-N-C, (c) In/Ni-N-C, and (d) In/NC catalysts.

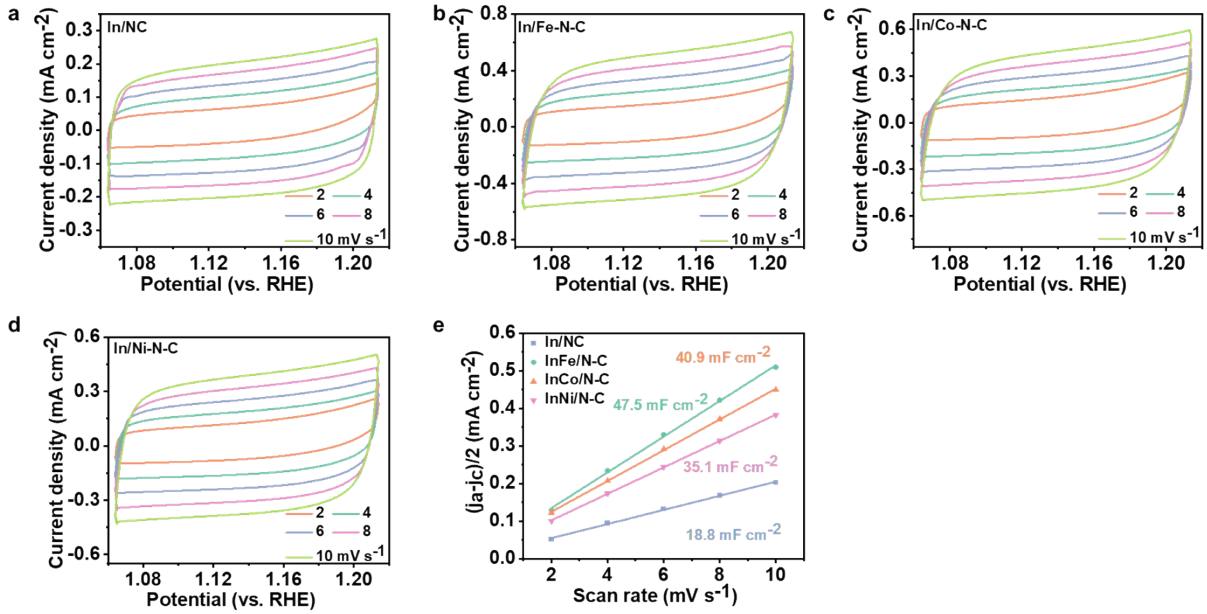

Figure S18 CV curves of (a) In/NC, (b) In/Fe-N-C, (c) In/Co-N-C, and (d) In/Ni-N-C catalysts. (e) Electrochemical double-layer capacitance (C_{dl}) of In/NC, In/Fe-N-C, In/Co-N-C and In/Ni-N-C catalysts.

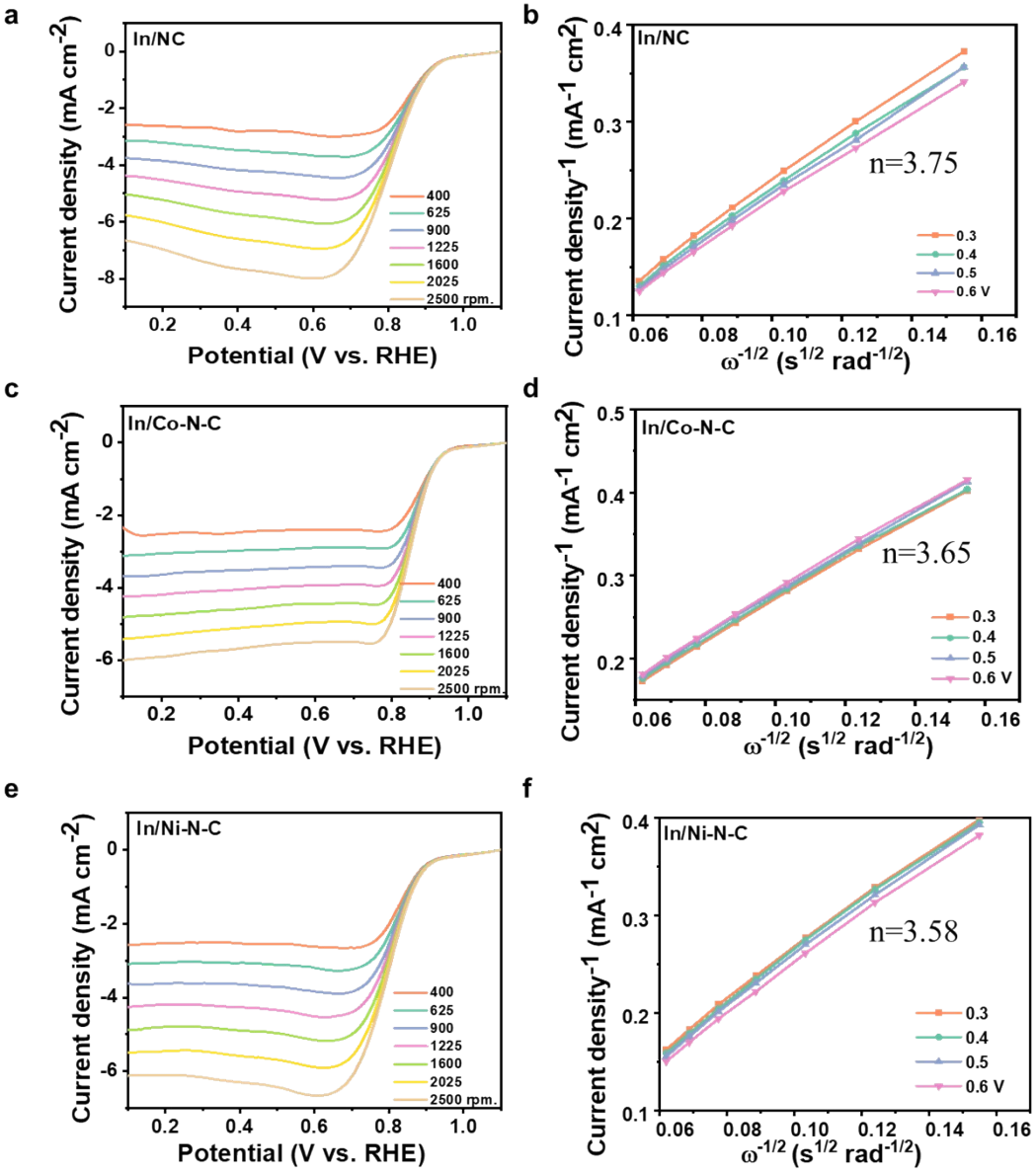

Figure S19 (a) ORR polarization curves of In/NC at different rotating speeds. (b) K-L plots and electron-transfer numbers. (c) ORR polarization curves of In/Co-N-C at different rotating speeds. (d) K-L plots and electron-transfer numbers. (e) ORR polarization curves of In/Ni-N-C at different rotating speeds (f) K-L plots and electron-transfer numbers.

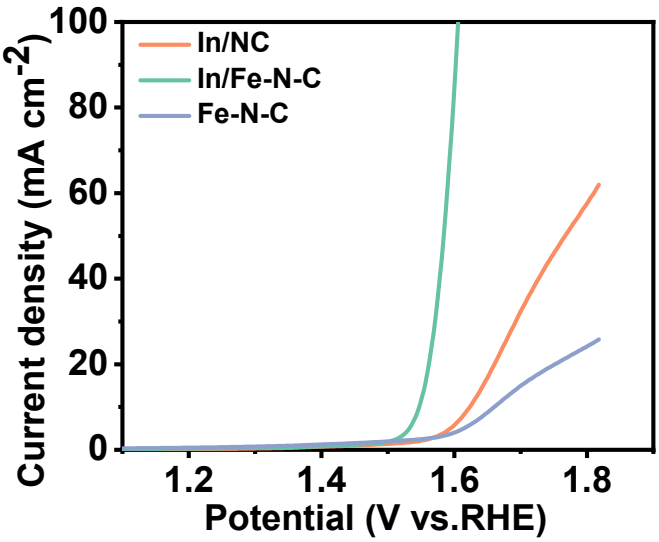

Figure S20 LSV curves for OER.

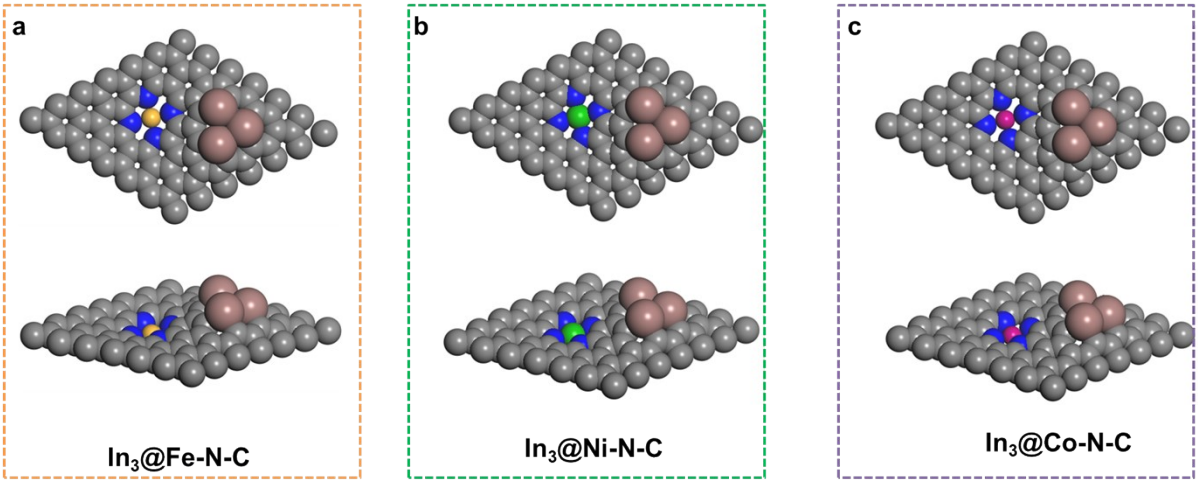

Figure S21 Illustration of atomic configurations for three types of local structures.

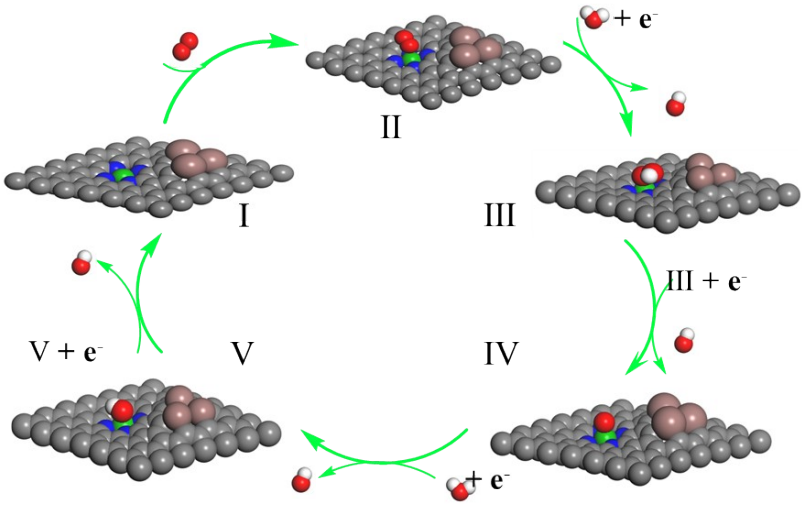

Figure S22 The proposed ORR mechanism diagram on In/Ni-N-C.

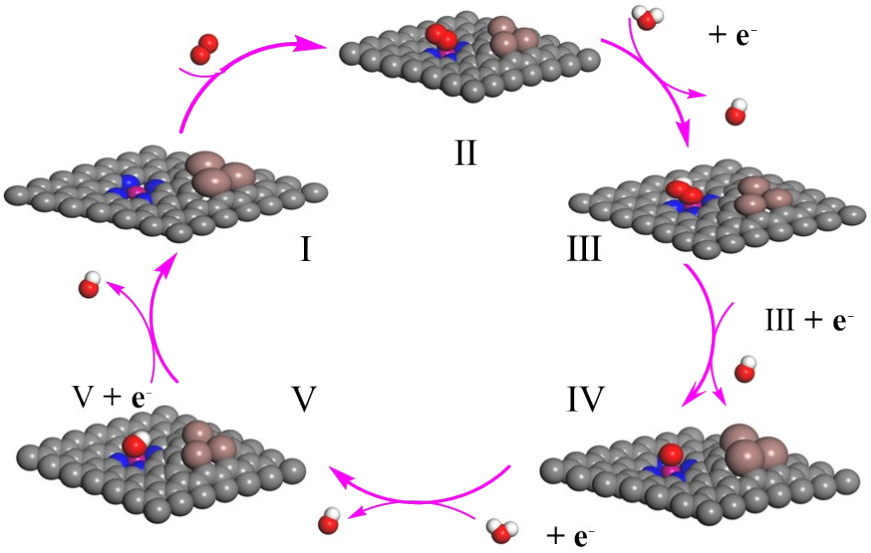

Figure S23 The proposed ORR mechanism diagram on In/Co-N-C.

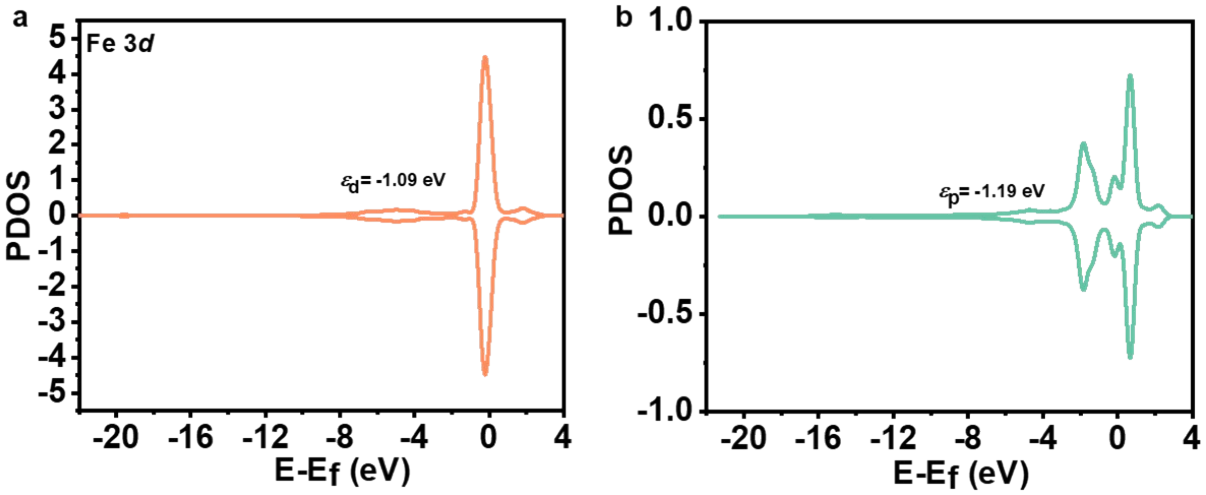

Figure S24 The PDOS curves for (a) Fe-N-C and (b) In_3-C.

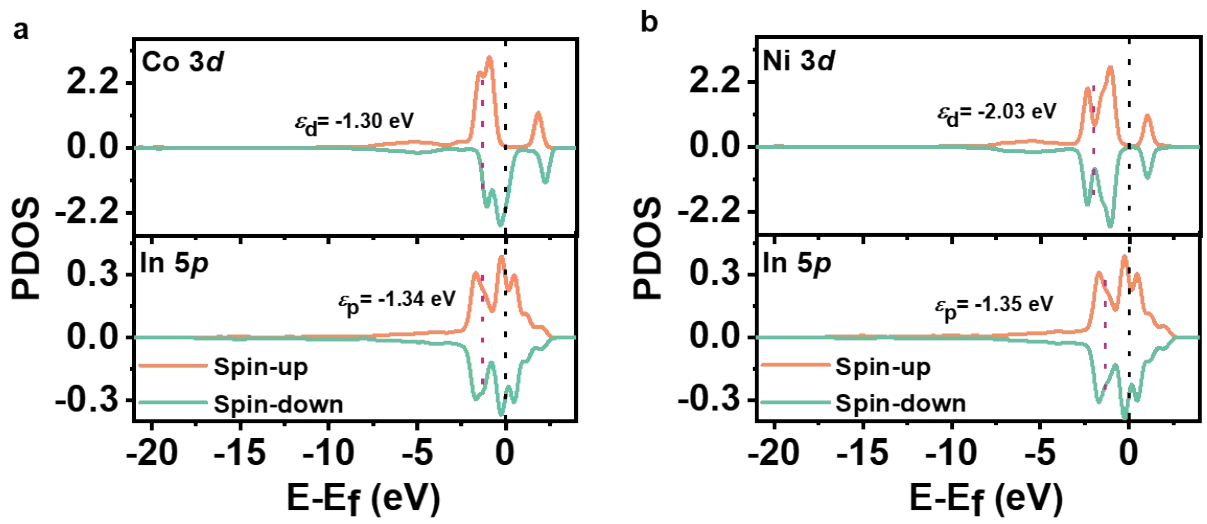

Figure S25 The PDOS curves for In/Co-N-C and In/Ni-N-C.

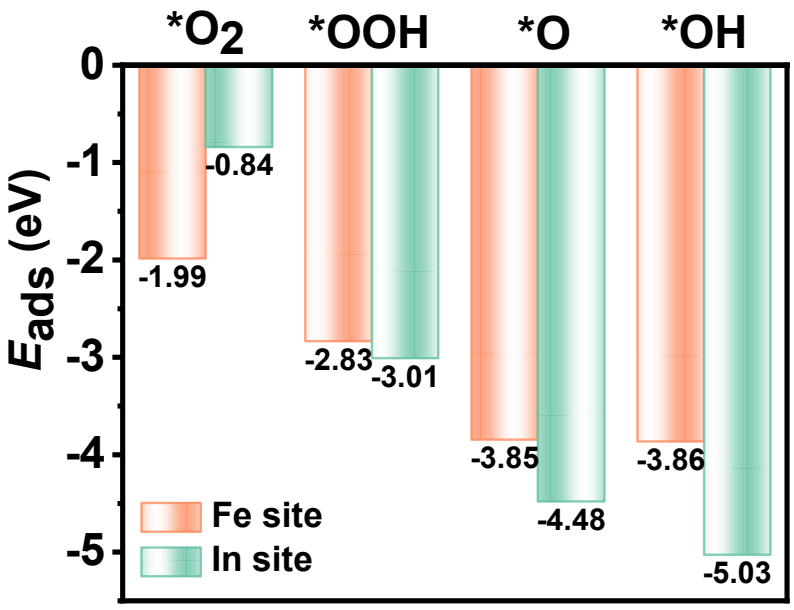

Figure S26 The adsorption energy with different oxygenated intermediates on Fe and In site in In/Fe-N-C.

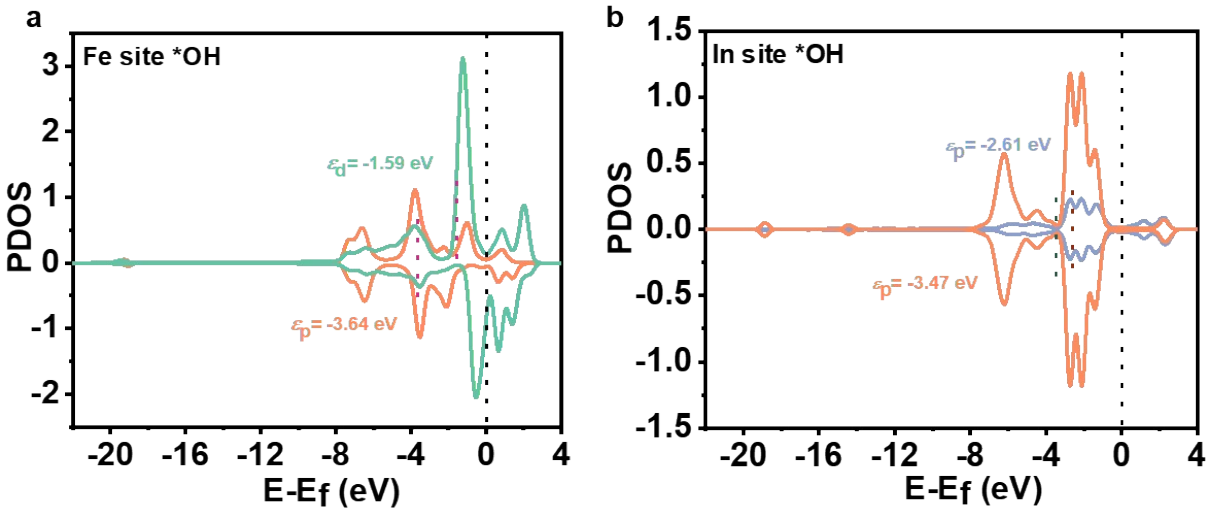

Figure S27 The PDOS curves for the adsorption of *OH on (a) Fe and (b) In site in In/Fe-N-C, respectively.

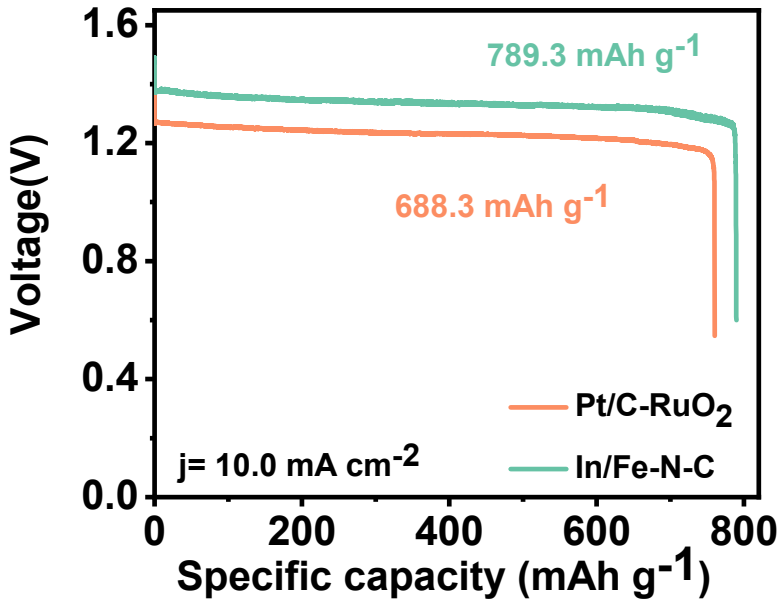

Figure S28 Specific capacities of aqueous ZABs at 10 mA cm^{-2} discharge current densities.

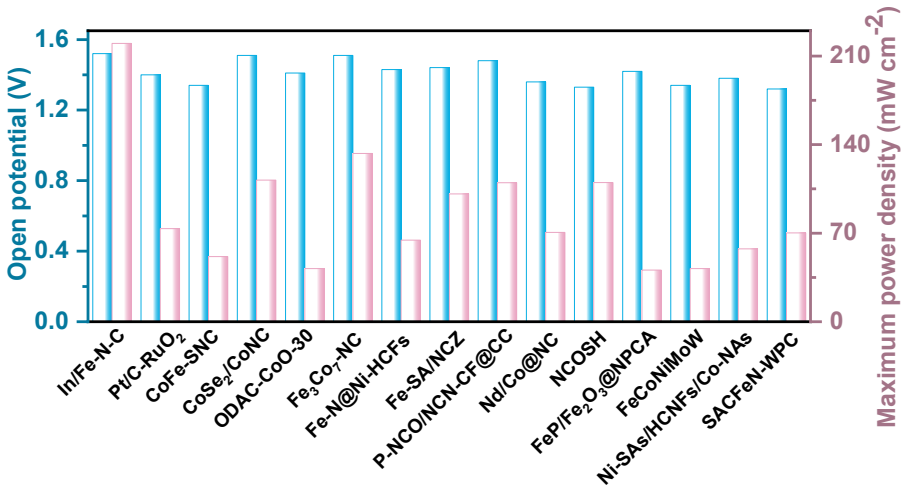

Figure S29 The performance comparison of solid-state ZABs with recently reported non-precious metal catalysts.

Table S1 The BET surface and pore volume of In/NC, In/Fe-N-C, In/Co-N-C, and In/Ni-N-C catalysts.

Catalyst	S_{BET} ($m^2 g^{-1}$)	Pore Volume ($cm^3 g^{-1}$)
In/NC	309.6	1.066
In/Fe-N-C	230.0	0.730
In/Co-N-C	177.0	0.604
In/Ni-N-C	149.4	0.515

Table S2 The element content of In/NC, In/Fe-N-C, In/Co-N-C and In/Ni-N-C catalysts from XPS results.

Catalyst	C (at.%)	N (at.%)	O (at.%)	In (at.%)	Fe/Co/Ni (at.%)
In/NC	83.61	6.22	9.12	1.05	/
In/Fe-N-C	83.68	6.78	8.41	0.72	0.41（Fe）
In/Co-N-C	82.80	6.92	8.95	1.09	0.24（Co）
In/Ni-N-C	83.85	6.42	8.20	1.32	0.21（Ni）

Table S3. The EXAFS fitting parameters at the Fe k-edge for Fe foil, and In/Fe-N-C (S_0^2 = 0.71).

Catalyst	Path	CN	R(Å)	σ^2(Å^2)	ΔE_0 (eV)	R factor
Fe foil	Fe-Fe1	6	2.85±0.01	0.00562	-1.58	0.008
	Fe-Fe2	8	2.47±0.01	0.00446		
In/Fe-N-C	Fe-N	3.7±0.2	2.00±0.01	0.00886	1.98	0.003

Table S4. The EXAFS fitting parameters at the In k-edge for In foil, and In/Fe-N-C (S_0^2 = 0.85).

Catalyst	Path	CN	R(Å)	σ^2(Å^2)	ΔE_0 (eV)	R factor
In foil	In-In1	4	3.10±0.01	0.0200	-1.50	0.006
	In-In2	8	3.29±0.01	0.0200	2.00	
In/Fe-N-C	In-In	9.0±1.8	3.31±0.01	0.0200	-10.0	0.009
	In-C	0.9±0.2	2.13±0.01	0.0200	3.00	

S_0^2 is the amplitude reduction factor, CN is the coordination number; R is the interatomic distance; ΔE_0 is the inner potential correction; σ^2 is Debye-Waller factor (a measure of thermal and static disorder in absorber-scatterer distances). R factor is used to value the fitting goodness.

Table S5 The comparison of ORR and OER performance for Fe-based single-atom catalysts.

Catalysts	E_{onset} (V vs. RHE)	$E_{1/2}$ (V vs. RHE)	J_L (mA cm^{-2})	η_{10} (mV vs. RHE)	Tafel (mV dec^{-1})	Ref.
In/Fe-N-C	1.05	0.92	5.76	318	52.3	This work
FeC/N-G-SA	N.A.	0.89	N.A.	370	73.0	[1]
P-doped Fe-N-C	N.A.	0.882	6.50	365	81.0	[2]
Fe-N/P-C-700	0.941	0.867	5.66	430	N.A.	[3]
SA-Fe-SNC@900	1.01	0.876	N.A.	402	N.A.	[4]
Fe-NSDC	0.96	0.84	N.A.	410	59.0	[5]
FeN_4CB	N.A.	0.84	5.58	350	N.A.	[6]
Fe/Ni-N-C	1.005	0.861	5.76	322	69.0	[7]
Ni-N_4/GHSs/Fe-N_4	0.93	0.83	N.A.	390	81.0	[8]
CoFe-SNC	0.97	0.86	5.50	490	78.7	[9]
FePc&rGO	0.98	0.89	5.40	N.A.	N.A.	[10]
Co-CoN_4@NCNs	0.91	0.83	N.A.	310	78.1	[11]
Fe-N@Ni-HCFs	N.A.	0.88	N.A.	337	54.7	[12]
Fe-SA/NCZ	1.00	0.87	N.A.	320	51.0	[13]

Table S6 The comparisons of aqueous ZABs performance for recently reported non-precious metal catalysts.

Catalysts	Specific capacity (mAh g^{-1})	Maximum power density (mW cm^{-1})	Cycling performance (h)	Ref.
In/Fe-N-C	789.6	318.2	1650 @10 mA cm^{-1}	This work
Co-CoN_4@NCNs	776.7	118.8	500 @10 mA cm^{-1}	[11]
NiFe-LDH/Fe1-N-C	N.A.	205.0	400 @2 mA cm^{-1}	[14]
FePc&rGO	739.7	103.0	133 @5 mA cm^{-1}	[10]
ODAC-CoO-30	N.A.	128.5	150 @5 mA cm^{-1}	[15]
CoFe-SNC	776.3	76.5	135 @10 mA cm^{-1}	[9]
FeP/Fe_2O_3@NPCA	717.0	130.0	160 @5 mA cm^{-1}	[16]
ZnSe@PNC-1000	818.0	126.0	200 @5 mA cm^{-1}	[17]
HfCo-N-C	795.0	184.0	N.A.	[18]
Ni-SAs/HCNFs/Co-NAs	N.A.	140.7	200 @10 mA cm^{-1}	[19]
Co-N,P-HCS	736.5	208.7	750 @5 mA cm^{-1}	[20]
CoP_3/CeO_2/C-2	767.7	150.0	120 @5 mA cm^{-1}	[21]
P/Fe-N-C	785.4	269.0	192 @10 mA cm^{-1}	[22]

Table S7 The comparison of solid-state ZAB performance.

Catalysts	Open-circuit voltage (V)	Maximum power density (mW cm^{-1})	Ref.
In/Fe-N-C	1.52	220.0	This work
Pt/C-RuO_2	1.40	73.6	This work
CoFe-SNC	1.34	51.5	[9]
$CoSe_2$/CoNC	1.51	112.0	[23]
ODAC-CoO-30	1.41	42.0	[15]
Fe_3Co_7-NC	1.51	133.0	[24]
Fe-N@Ni-HCFs	1.43	64.5	[12]
Fe-SA/NCZ	1.441	101.0	[13]
P-NCO/NCN-CF@CC	1.48	109.8	[25]
Nd/Co@NC	1.36	70.6	[26]
NCOSH	1.33	110.0	[27]
FeP/Fe_2O_3@NPCA	1.42	40.8	[16]
FeCoNiMoW	1.34	42.05	[28]
Ni-SAs/HCNFs/Co-NAs	1.38	57.6	[19]
SACFeN-WPC	1.32	70.2	[29]

References

1. Xiao, M.; Xing, Z.; Jin, Z.; Liu, C.; Ge, J.; Zhu, J.; Wang, Y.; Zhao, X.; Chen, Z.. *Adv. Mater.* 2020, **32**, 2004900.

2. Sheng, J.; Sun, S.; Jia, G.; Zhu, S.; Li, Y. *ACS nano* 2022, **16**, 15994-16002.

3. Yuan, K.; Lützenkirchen-Hecht, D.; Li, L.; Shuai, L.; Li, Y.; Cao, R.; Qiu, M.; Zhuang, X.; Leung, M. K. H.; Chen, Y. et al. *J. Am. Chem. Soc.* 2020, **142**, 2404-2412.

4. Chen, Z.; Peng, X.; Chen, Z.; Li, T.; Zou, R.; Shi, G.; Huang, Y.; Cui, P.; Yu, J.; Chen, Y. et al. *Adv. Mater.* 2023, **35**, 2209948.

5. Zhang, J.; Zhang, M.; Zeng, Y.; Chen, J.; Qiu, L.; Zhou, H.; Sun, C.; Yu, Y.; Zhu, C.; Zhu, Z. *Small* 2019, **15**, 1900307.

6. Zhao, X.; Li, X.; Bi, Z.; Wang, Y.; Zhang, H.; Zhou, X.; Wang, Q.; Zhou, Y.; Wang, H.; Hu, G. *J. Energy Chem.* 2022, **66**, 514-524.

7. Li, H.; Wang, J.; Qi, R.; Hu, Y.; Zhang, J.; Zhao, H.; Zhang, J.; Zhao, Y. *Appl. Catal. B Environ.* 2021, **285**, 119778.

8. Chen, J.; Li, H.; Fan, C.; Meng, Q.; Tang, Y.; Qiu, X.; Fu, G.; Ma, T. *Adv. Mater.* 2020, **32**, 1900307.

9. Weng, C.-C.; Ren, J.-T.; Wang, H.-Y.; Lv, X.-W.; Song, Y.-J.; Wang, Y.-S.; Chen, L.; Tian, W.-W.; Yuan, Z.-Y. *Appl. Catal. B Environ.* 2022, **307**, 121190.

10. Mei, Z.-y.; Cai, S.; Zhao, G.; Jing, Q.; Sheng, X.; Jiang, J.; Guo, H. *Energy Storage Mater.* 2022, **50**, 12-20.

11. Ding, K.; Hu, J.; Luo, J.; Zhao, L.; Jin, W.; Liu, Y.; Wu, Z.; Zou, G.; Hou, H.; Ji, X. *Adv. Func. Mater.* 2022, **32**, 2207331.

12. Tian, Y.; Wu, Z.; Li, M.; Sun, Q.; Chen, H.; Yuan, D.; Deng, D.; Johannessen, B.; Wang, Y.; Zhong, Y. et al. *Adv. Func. Mater.* 2022, **32**, 2209273.

13. Jin, Z.; Jiao, D.; Dong, Y.; Liu, L.; Fan, J.; Gong, M.; Ma, X.; Wang, Y.; Zhang, W.; Zhang, L. et al. *Angew. Chem. Int. Ed.* 2023, **63**, e202318246.

14. Liu, Z. Q.; Liang, X.; Ma, F. X.; Xiong, Y. X.; Zhang, G.; Chen, G.; Zhen, L.; Xu, C. Y. *Adv. Energy Mater.* 2023, **13**, 2203609.

15. Tian, Y.; Liu, X.; Xu, L.; Yuan, D.; Dou, Y.; Qiu, J.; Li, H.; Ma, J.; Wang, Y.; Su, D. et al. *Adv. Func. Mater.* 2021, **3**1, 2101239.

16. Wu, K.; Zhang, L.; Yuan, Y.; Zhong, L.; Chen, Z.; Chi, X.; Lu, H.; Chen, Z.; Zou, R.; Li, T. et al. *Appl. Catal. B Environ.* 2022, **307**, 121190.

17. Yang, L.; Yao, X.; Du, C.; Han, Z.; Jin, M.; Peng, S.; Ma, X.; Zhu, Y.; Zou, M.; Cao, C. Constructing delocalized electronic structures to motivate the oxygen reduction activity of zinc selenide for high-performance zinc-air battery. *Adv. Mater.* 2020, **32**, 2002292.

18. Duan, D.; Huo, J.; Chen, J.; Chi, B.; Chen, Z.; Sun, S.; Zhao, Y.; Zhao, H.; Cui, Z.; Liao, S. *Chem. Eng. J.* 2024, **481**, 148598.

19. Chen, Y.; Qiao, S.; Tang, Y.; Du, Y.; Zhang, D.; Wang, W.; Zhang, H.; Sun, X.; Liu, C. *Small* 2024, **20**, 2310491.

20. Wang, X.; Zhou, X.; Li, C.; Yao, H.; Zhang, C.; Zhou, J.; Xu, R.; Chu, L.; Wang, H.; Gu, M. et al. *ACS nano* 2022, **16**, 15273-15285.

21. Li, J.; Kang, Y.; Lei, Z.; Liu, P. *Adv. Mater.* 2022, **34**, 2204021.

22. Zhou, Y.; Lu, R.; Tao, X.; Qiu, Z.; Chen, G.; Yang, J.; Zhao, Y.; Feng, X.; Müllen, K. *Appl. Catal. B Environ.* 2023, **321**, 122029.

23. Xu, Q.; Peng, L.; Luo, K.; Zhong, J.; Zhang, C.; Yuan, D. *J. Am. Chem. Soc.* 2023, **145**, 3647-3655.

24. Gu, T.; Zhang, D.; Yang, Y.; Peng, C.; Xue, D.; Zhi, C.; Zhu, M.; Liu, J. *J. Colloid Interface Sci.* 2023, **643**, 73-81.

25. Liu, Y.; Jiang, Z.; Jiang, Z. J. *Adv. Func. Mater.* 2022, **33**, 2212299.

26. Fan, C.; Wang, X.; Wu, X.; Chen, Y.; Wang, Z.; Li, M.; Sun, D.; Tang, Y.; Fu, G. *Adv. Func. Mater.* 2023, **33**, 2302883.

27. Zheng, X.; Cao, Y.; Wu, Z.; Ding, W.; Xue, T.; Wang, J.; Chen, Z.; Han, X.; Deng, Y.; Hu, W. *Adv. Energy Mater.* 2022, **13**, 2203244.

28. He, R.; Yang, L.; Zhang, Y.; Jiang, D.; Lee, S.; Horta, S.; Liang, Z.; Lu, X.; Ostovari Moghaddam, A.; Li, J. et al. *Adv. Energy Mater.* 2022, **12**, 2103275.

29. Zhong, L.; Jiang, C.; Zheng, M.; Peng, X.; Liu, T.; Xi, S.; Chi, X.; Zhang, Q.; Gu, L.; Zhang, S. et al. *ACS Energy Letters* 2021, **6**, 3624-3633.